

Division - Soil Processes and Properties | Commission - Soil Mineralogy

Origin and properties of kaolinites from soils of a toposequence in Southern Brazil

Daniela Nicole Ferreira^(1,2) , **Vander de Freitas Melo**⁽²⁾ , **Samara Alves Testoni**⁽³⁾ , **Pablo Vidal-Torrado**⁽⁴⁾  and **Jairo Calderari de Oliveira Junior**^{(2)*} ⁽¹⁾ Instituto Água e Terra do Paraná, Setor de Licenciamento Florestal, Curitiba, Paraná, Brasil.⁽²⁾ Universidade Federal do Paraná, Departamento de Solos, Curitiba, Paraná, Brasil.⁽³⁾ Universidade Federal do Rio Grande do Sul, Campus do Vale, Porto Alegre, Rio Grande do Sul, Brasil.⁽⁴⁾ Universidade de São Paulo, Escola Superior de Agricultura Luiz de Queiroz, Departamento de Ciência do Solo, Piracicaba, São Paulo, Brasil.

ABSTRACT: Kaolinite is the main clay mineral in most soils around the world and has been widely used for industrial purposes. This research aimed to study chemical, morphological and crystallographic characteristics of kaolinite, and establish the origin of kaolinitic samples on Serra do Mar and kaolinitic layers on peatlands, located at Southern Brazil. Samples were collected on different geomorphological positions: two samples at Serra do Mar (kaolinitic saprolite - SAP, and kaolinitic layers - KL); and two cores at the peatland with Sapric Histosols from Quaternary sedimentary basin. Granulometry and total organic carbon (TOC) were determined in soil samples. Kaolinite in silt and clay fractions was studied by chemical extractions, X-ray diffraction (XRD), thermal analysis (DTA/TG), and scanning electron microscopy with energy dispersive spectroscopy - SEM/EDS. Chemical and mineralogical characteristics of kaolinite were divided into two groups, according to the particle size and the location of the deposit in the relief. Silt fraction: i) SAP - genesis mainly derived from mica weathering; ii) peatland, containing pseudomorph crystals smaller than those found in Serra do Mar; Clay fraction: i) Serra do Mar - there was a larger contribution of K-feldspar weathering in the genesis of kaolinite from KL in relation to SAP; ii) peatland - the stronger weathering and the hydromorphic conditions resulted in less neoformed crystalline kaolinites. For both environments, the substitution of Al³⁺ by Fe³⁺ into the octahedral sheet led to a reduction in the mineral thickness and also increased the occurrence of structural deformations in clay kaolinite. Kaolinite in peatland is a combination of the following genesis processes: transportation from Serra do Mar (mainly in the silt fraction) and; formation in situ through neogenesis process (dominant in the clay fraction).

Keywords: kaolinite, isomorphic substitution, mica, X-ray diffraction, SEM-EDS.

* **Corresponding author:**
E-mail: calderari@ufpr.br

Received: March 28, 2023

Approved: October 27, 2023

How to cite: Ferreira DN, Melo VF, Testoni AS, Vidal-Torrado P, Oliveira Junior JC. Origin and properties of kaolinites from soils of a toposequence in Southern Brazil. Rev Bras Cienc Solo. 2024;48:e0230028.

<https://doi.org/10.36783/18069657rbc20230028>

Editors: José Miguel Reichert  and Alberto Vasconcellos Indá Júnior .

Copyright: This is an open-access article distributed under the terms of the Creative Commons Attribution License, which permits unrestricted use, distribution, and reproduction in any medium, provided that the original author and source are credited.



INTRODUCTION

Kaolin layers and deposits are widely employed for industrial purposes (Pruett, 2016; Bedassa et al., 2019; Sharaka et al., 2022), and the mineral is economically relevant in the manufacture of several products such as paper and paint pigments, functional fillers for rubber, plastics, ink, raw materials for ceramics, fiberglass, and cement (Mártires, 2006; Campos and Farias, 2017). Kaolinite is one of the six most abundant minerals in the earth's crust, and its genesis is known as primary or secondary (Gaudin et al., 2020; Karakaya et al., 2021). Primary kaolinite is derived from *in situ* weathering, with hydrothermal alterations or residual accumulations from the weathering process, while secondary kaolinite is derived from transportation and deposition processes of clasts or from sedimentation materials with reduced size (Górniak, 1997; Ouyang et al., 2021).

Kaolinite layers and deposits can be found in numerous countries around the world: United States (Hinckley, 1962; Pruett, 2016), Turkey (Sayin, 2007), Pakistan (Ismail et al., 2014), Africa (Ekosse, 2010), Germany (Gilg et al., 2003), Asia (Chen et al., 1997) and South America (Dill et al., 1997; Montes et al., 2002; Wilson et al., 2006). Brazil assumes a prominent position in the occurrence of kaolin deposits (Pruett, 2016) and produced about 1.8 million of tons of beneficiated kaolinite in 2020 (Departamento Nacional de Produção Mineral, 2021).

Kaolinite mineral deposits and its mining in the Paraná State are associated with rocks from the crystalline basement (Serra do Mar) and sedimentary basin of Upper Iguazu Plateau. The first location present granite-gneiss-migmatite complex (Salamuni et al., 2003; Baioumy, 2014; Batista et al., 2018) and occurs at Serra do Mar, in the highest level, with common orographic rains exceeding 2,500 mm per year (Alvares et al., 2013). These environmental conditions lead to an intensive alteration of the rocks via desilication, favoring the weathering of feldspars/mica and the neogenesis of kaolinite deposits (Driese et al., 2007; Ouyang et al., 2021). Toward to the east, hilly zones with elongated and planar tops made up the Curitiba and Upper Iguazu Plateau, with altitude varying from 800 to 1100 m a.s.l., with some remnants of crystalline basement and claystone named Guabirotuba Formation, dated from Quaternary-Miocene-Pleistocene (Salamuni et al., 2003). In the lowest position of the landscape, peatlands originated (Upper Iguazu Plateau), with plains and alluvial terrains made up of sediments dated from Quaternary (Salamuni et al., 2003). In both Curitiba and Upper Iguazu Plateaus, sediments are granulometric and compositional unripe, typical of environments with material transported along short distances (Vieira and Fernandes, 2020).

Hypothesis about the formation of kaolinite layers in nearby peatlands have also been reported: i) The process of desilication of rocks comes from a preterit environment with predominant acidic conditions and high levels of organic matter, which are interlayered with kaolin in floodplain areas commonly classified as Histosols (*Organossolos*) (Biondi and Santos, 2004). In this way, the weathering of primary minerals transported along the relief quotes forms the primary kaolin deposit; ii) The presence of a well-drained environment with higher levels of Fe oxides associated with sediment transportation and deposition processes were fundamental to form the secondary kaolin deposits (Oliveira Junior et al., 2010; Mucha, 2020). These studies raise questions about the relevance of the genesis of kaolinite layers, and how these processes can be associated with the relief and the landscape modeling in Serra do Mar and peatland areas).

This research aimed to study chemical, morphological and crystallographic kaolinite properties and establishing the origin of kaolinitic deposits on Serra do Mar and kaolinitic layers on peatlands, Southern Brazil. We hypothesized that the characteristics of kaolinite from Serra do Mar and peatlands have similarities, which may reveal an associated genesis of the mineral in these two relief positions.

MATERIALS AND METHODS

Sampling area

To assess the hypothesis of transported material from Serra do Mar to peatland (secondary kaolinite), samples were collected in two different geomorphological positions (Figure 1):

i) Peatland: situated on the Quaternary sedimentary basin (Upper Iguaçú Plain - Figure 2a). Two cores of 6 m depth were sampled in this area (25° 55' 28.47" S; 49° 12' 1.95" W, 925 m a.s.l.) located among Serra do Mar and Curitiba Plateau. Upper Iguaçú Plain has extensive areas of peatlands, formed within the trans-Amazonian gneisses and migmatites of the coastal complex, which are filled by sediments derived from the Serra do Mar (Salamuni et al., 2003). Soils derived from peatlands were classified as Sapric Histosol (Mucha, 2020), which corresponds to *Organossolo Háplico Sáprico* (Santos et al., 2018). To collect randomly layers, the peat bog depth was determined using a 6 m stake in transects spaced around 10 m between each other, and the coordinates were recorded (Figure 1c). Stakes were inserted into Histosols until there was great resistance to penetration, being considered the base of the sedimentation basin. The CAD software was used to calculate the peat volume, interpolating the data yielded at each point of the transects (Figure 1c). Core sampling was located in the deepest peat bog (Figure 1c). Two sampling points (C1 and C2) were selected 30 m apart from each other, and the soil samples were collected using vibracore to reduce the compaction process. In this sampling, a motor is used to produce a high frequency under low amplitude vibration, which is transferred to a tube that penetrates the ground. This vibration reduces the attrition between the tube and the sample and also reduces the sample compaction. Samples inside the probe were sectioned every 5 cm.

ii) Serra do Mar: located at the upper position on the landscape, with altitude ranging from 950 to 1,400 m a.s.l. Two samples were collected on this geomorphological position - one derived from Saprolite of Crystalline rocks (kaolinitic saprolite - SAP) - directly formed by the alteration of the rock, without transportation (Figure 2b), and one derived from kaolinitic deposit - KD, in the toeslope, considering in situ formation or very short distance of transportation (Figure 2c) (coordinates 25° 34' 53.67" S; 48° 59' 00.71" W, 980 m of altitude a.s.l.). Relative positions of peatland and Serra do Mar areas are presented in figure 1b. The SAP site has common features and represents the various types of saprolite in Serra do Mar. Also, the sampling was favoured due to the exposure of the saprolite and deposit through the cut slope. Vegetation of Serra do Mar is classified as Mixed Ombrophilous Forest, while the lowland has a mixture of *Sphagnum* spp. and graminoid species. Climate is classified in both areas as Cfb mesothermal humid subtropical, according to Köppen classification system.

Total carbon content and particle size analyses

Total carbon and nitrogen contents were obtained via dry combustion with the equipment Elementar Vario EL III. Soil organic material was removed by H₂O₂ 30 % (v/v) in a water bath at 60 °C, and samples were dispersed with NaOH 0.5 mol L⁻¹. Sand fraction was retained in 0.05 mm sieve mesh while silt and clay contents were obtained by pipette method (Gee and Bauder, 1979) (Table 1).

Mineralogical analysis

Samples recovered from the tube were clustered based on total C contents lower than 4 % associated with light colorations (white, grey, or light brown) (Figure 3), and then were selected for particle size and mineralogical analyses. A total of 43 mineral subsamples with light colorations were collected, forming six composite samples, each one representing a layer of kaolinite in peatland (Figure 3). These layers were identified according to the sampling core and the mean depth. For example, sample C1-145 refers to Core 1 and mean depth of 1.45 m (layer from 1.20 to 1.50 m).

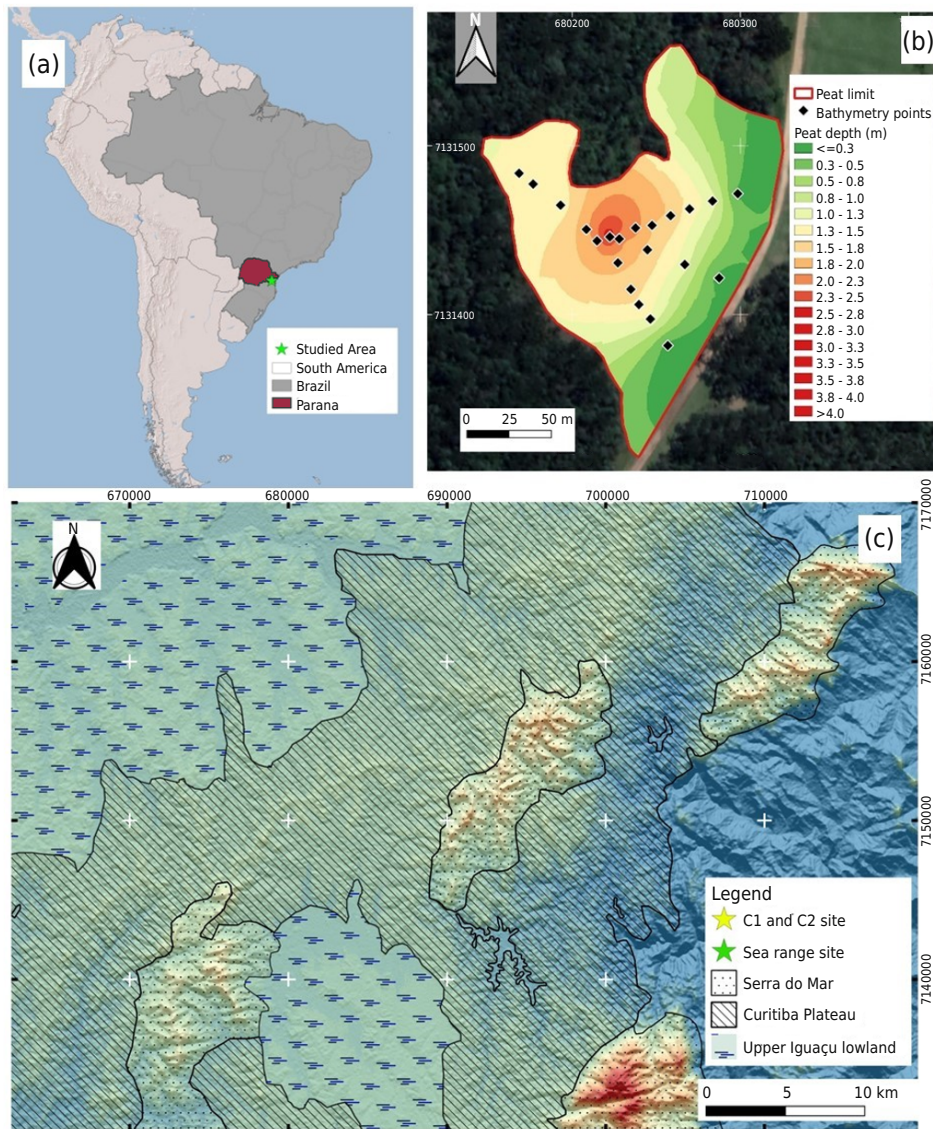


Figure 1. Map Brazil, Paraná State and study area (a); perimeter of the peat bog area, points used in depth determination and interpolated peat depths values (b); location of both studied areas in lowland and Serra do Mar in different geomorphological units (c).

Soil samples were treated with H_2O_2 30 % (v/v) and NaOH 0.5 mol L^{-1} and silt and clay fractions, after sieving at 0.05 mm sieve mesh, were separated by sedimentation procedures, according to Stoke's law (Jackson, 1979; Ciotta et al., 2003). Clay fraction was frozen for 30 days and then freeze-dried.

Silt and clay fractions were analyzed by X-ray diffraction (XRD) via oriented samples. The XRD patterns were obtained by Panalytical X'Pert3 device, under a speed of $0.42 \text{ }^\circ 2\theta \text{ s}^{-1}$. Diffractometer was equipped with a graphite monochromator system, and used a $\text{CuK}\alpha$ radiation, operated at 40 kV and 40 mA . The following crystallographic kaolinite parameters were obtained in the clay fraction, using Si standard to correct the instrumental distortions (Gruner, 1932; Brindley and Robinson, 1945; Klug and Alexander, 1974; Hughes and Brown, 1979): 001 d -spacing; structural deformations (microstrain-ms); mean crystal diameter (MCD) from the full width at half height (FWHM) of the reflections (001), (020), and (060) (Scherrer equation); asymmetry index (AI) according to the plane (001) and; "crystallinity index" of Hughes and Brown (HBCI).

Pedogenic Fe iron oxides were removed from the clay and silt fractions using sodium dithionite–citrate–bicarbonate (DCB) method (Mehra and Jackson, 1958). Deferrified clay and silt samples were subjected to two washes with 80 mL of $(\text{NH}_4)_2\text{CO}_3$ 0.5 mol L^{-1} ,

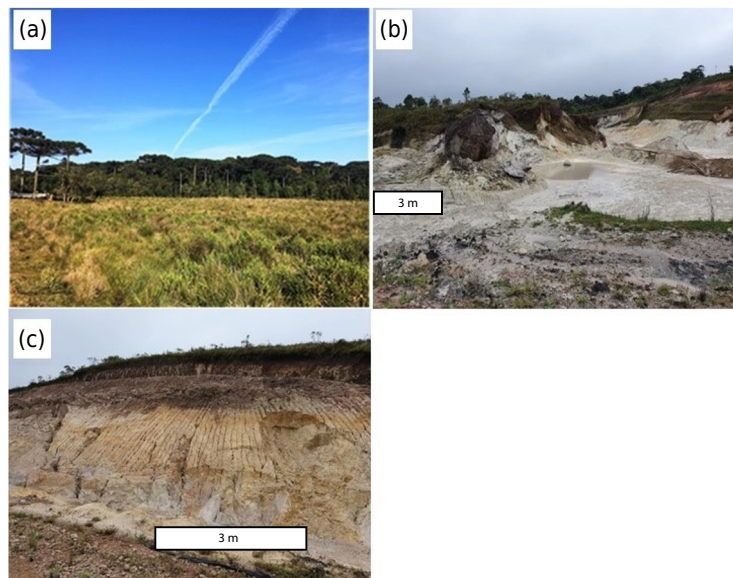


Figure 2. Lowland Histosol area (a); kaolinitic layer(KL) on Serra do Mar (b); kaolinitic saprolite (SAP) on Serra do Mar (c). The white box represents approximately 3 m in the field.

and one with 80 mL of deionized water to remove salt excess. The mass reduction was calculated from the difference between the initial and the final sample weight after DCB extraction. Simultaneous differential thermal and thermogravimetry analyses (DTA/TG) of the deferrified clay samples were processed in a Shimadzu equipment and DTG-60 model. Quantitative analysis was processed based on mass loss of kaolinite and gibbsite by TG. Samples were heated at room temperature to 950 °C in a platinum crucible, at a heating rate of 10 °C min⁻¹ and nitrogen gas flow of 50 mL min⁻¹. Kaolinite and gibbsite contents of the deferrified samples were corrected using the sample mass reduction in the DCB extraction. Subsequently, additional treatments with K⁺, Mg²⁺ and ethylene glycol saturation and heating were performed on deferrified clay fraction (Whittig and Allardice, 1986) to differentiate secondary 2:1 clay minerals.

Scanning Electron Microscopy with Energy Dispersive X-ray Spectroscopy

To assess morphology features and semi-quantitative chemical compositions of the mica pseudomorphs kaolinite particles in the silt fraction, samples C1-292, C2-315, C2-382 and SAP were selected based on silt XRD patterns for analysis via Scanning Electron Microscopy with Energy Dispersive X-ray Spectroscopy (SEM-EDS). Equipment Tescan Vega3 LMU operated at 20 kV and was equipped with an EDS system Oxford coupled to AZ Tech Advanced software. Samples from peatlands were selected based on the higher HBCI.

Table 1. Particle size analysis of kaolinitic saprolite (SAP) and kaolinitic layer (KL) on Serra do Mar and core samples from lowland Histosols (C1 and C2)

Sample	Sand	Silt	Clay	Silt/Clay	Texture
SAP	206	573	221	2.59	Silt loam
KL	304	488	208	2.35	Loam
C1-145	89	451	460	0.98	Silt clay
C1-172	63	573	364	1.57	Silt clay loam
C1-292	124	515	361	1.43	Silt clay loam
C2-130	101	494	405	1.22	Silt clay
C2-315	282	465	253	1.84	Loam
C2-382	44	472	484	0.98	Silt clay

Statistical analyses

Data from clay and silt fractions were assessed by multivariate analyses with “R Studio” software (RStudio, Boston, MA, USA). Principal Component Analysis (PCA) transforms a set of data into linear combinations, allowing to compare values with different scales and reducing numerical distance among variables. For multivariate analyses, original dataset was transformed through linear combinations and variance and covariance matrixes.

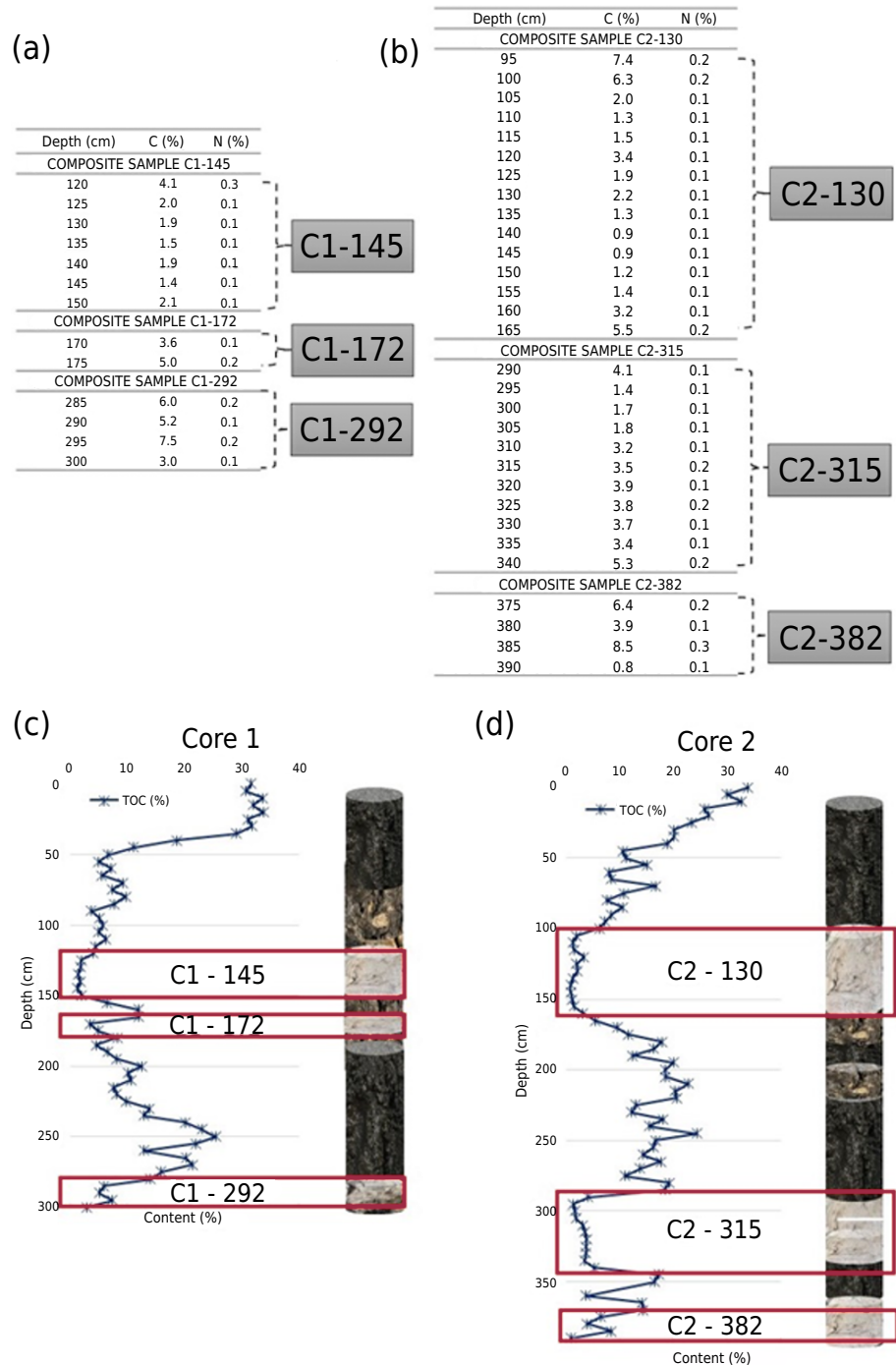


Figure 3. Sampling depth, total organic carbon and nitrogen contents of the samples collected on lowland Histosol (a, b); Mean total organic carbon (TOC) according to the sampling depths and sample colors (c, d).

RESULTS

It was observed alternated layers of kaolin and organic material along the sections of the sampling cores (different total organic carbon, clay, silt and sand contents and sample colors - Figure 3 and Table 1). The SAP and KL samples presented lower clay contents and higher silt/clay ratios, revealing incipient weathering of the parent material. Clay content does not present a trend in the core samples, which are related to differences in the deposition processes (Table 1).

Clay fraction of all samples is essentially kaolinitic (Table 2 and Figure 4). The highest kaolinite contents were found in Core 2 (C2-130) and the lowest contents in C1-172 sample (845 and 504 g kg⁻¹, respectively) (Table 2). Gibbsite was not identified in clay fraction of SAP and KL samples, and the highest content was found in the C2-130 (127 g kg⁻¹). Pedogenic Fe extracted by DCB was very low and was not identified in SAP, C1-292, C2-145 and C2-382 (Table 2). Iron content in the KL showed 0.3 g kg⁻¹ and the highest value was found in C1-172 (9.1 g kg⁻¹). From the XRD data (Figure 4), peaks at 1.4 and 0.72 nm were attributed to expansive 2:1 phyllosilicates and kaolinite 001 basal reflections, respectively. Furthermore, the asymmetry for lower 2θ angles observed in the 1.4 nm reflection is typical of interstratified kaolinite-smectite, as already reported in previous studies (Simas et al., 2006; Neumann et al., 2011; Testoni et al., 2017). Based on the shape and average position of the peaks, we obtained the following crystallographic parameters for kaolinite: MCD (Mean Crystal Dimension), ANL (Average Number of Layers), FWHH (Full Width at Half Height), and AI (Asymmetry Index).

Based on SEM silt images, silt crystals with planar growth were identified, typically found in phyllosilicate minerals such as kaolinite (Figure 5). The mean SiO₂/Al₂O₃ ratios obtained via EDS analysis for mica-kaolinite pseudomorphs (pointed out by red arrows in Figure 5) were the following: SAP - 1.67; C1-292 - 1.38; C2-315 - 1.37 and; C2-382 - 1.18 (Figure 6). Additionally, potassium showed higher contents in SAP samples and similar contents in floodplain samples.

The highest values of HBCI followed the lowest AI, except for the kaolinite in the clay fraction of SAP samples (Table 3). Additionally, kaolinite in clay fraction of SAP presented higher AI, suggesting higher 2:1 interstratification (AI = 0.213) than in KL samples (AI = 0.075), denoting larger content of pseudomorph crystals and incipient weathering of the parent material. Higher values of AI indicate a small dimension of the clay mineral crystals or structural disorders of kaolinite due to the presence of 2:1 interlayered minerals, such as kaolinite-smectite or kaolinite-hydroxy-Al interlayered smectite, since interstratified kaolinite-vermiculite is rarely found in most of the soils (Testoni et al., 2017).

Table 2. Contents of gibbsite (Gb) and kaolinite (Kt) obtained by DTA/TGA and pedogenic Fe oxides (Fe₂O₃ DCB) in the clay fraction

Sample	Gb	Kt	Fe ₂ O ₃ DCB ⁽¹⁾
SAP ⁽²⁾	nd	549	0.0
KL ⁽³⁾	nd	676	0.3
C1-145	78	764	0.0
C1-172	48	504	9.1
C1-292	91	731	4.4
C2-130	127	845	0.0
C2-315	112	799	0.4
C2-382	76	814	0.0

DTA/TGA: differential thermogravimetry analysis; DCB: sodium dithionite-citrate-bicarbonate method. ⁽¹⁾ Pedogenic Fe₂O₃ assessed by DCB extraction, ⁽²⁾ SAP: kaolinitic saprolite on Serra do Mar; and ⁽³⁾ KL: kaolinitic layer on Serra do Mar.

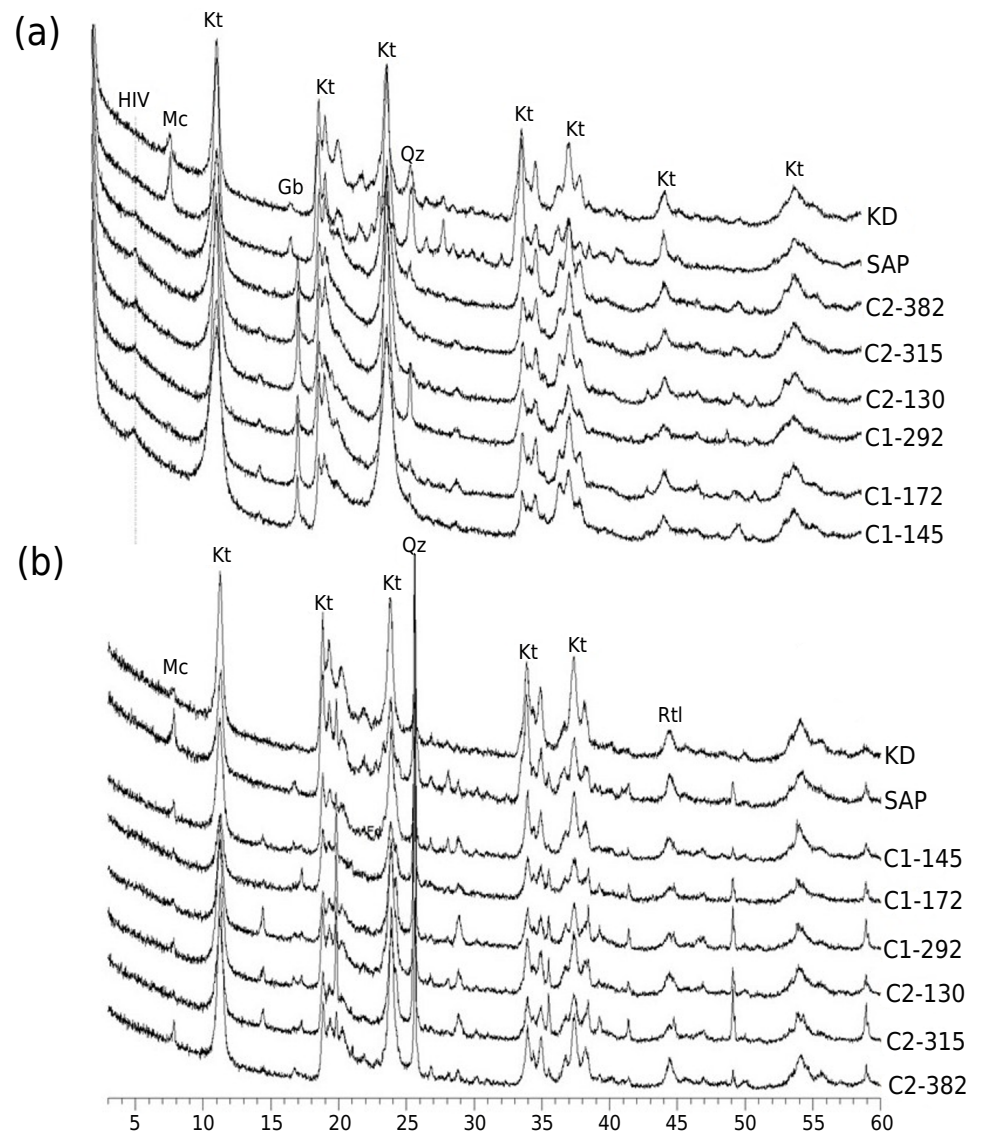


Figure 4. X-ray diffractogram patterns of oriented samples from Serra do Mar and floodplain Histosols (Core 1 and 2): clay (a) and silt (b) fractions. Mc: mica; HIV: hydroxy-interlayered vermiculite; Kt: kaolinite; Qz: quartz; Rt: rutile; and Gb: gibbsite.

It was observed a negative association between microstrain [ms (060)] and HBCI (Figure 7a), related to the poor ordering of kaolinite with high isomorphous substitution of Al^{3+} by Fe^{3+} into octahedral sheet, which also increase the unit cell dimension (Figure 7b). The highest values for ms were observed for Core 1 samples (C1-172 = 0.52) (Table 3), and the highest values of MCD (001) were found for C2-382, followed for KL and SAP (13.1, 11.0, and 10.0, respectively), while the other samples showed MCD near to 9.0 (Table 3). Asymmetry index and HBCI did not show correlation among the samples; however, it was found high values of HBCI for Serra do Mar samples (superficial samples of C1 and all C2 samples), while the lowest values of AI were found for SAP samples (C2-130 and C2-382, the uppermost and the deepest samples, respectively).

In PCA analysis, the first and second axes explain about 68.0 % of the total variability of the data set in the clay fraction (Figure 8a). The first axis opposes the contents of gibbsite and kaolinite to the HBCI of kaolinite in the clay fraction, representing the desilication process in the mineral contents and the variation of crystallographic characteristics of the kaolinite (46.1 % of all variation). The factorial axis 2 explains 32.3 % of the data variation, opposing the AI (001) and MCD (001) and revealing differences in the kaolinite

growth (KL opposite side of SAP) (Figure 8b). The first PCA axis for the silt fraction includes 68.0 % of the total variability of the data and opposes the HBCI and Al and Fe contents from DCB extraction (Figure 8c). Sample from Serra do Mar (KL) were closer to C2-382 and opposed to C1-172 and C1-292 in the first axis.

DISCUSSION

All sampled sites showed high kaolinite contents (Table 2). Migmatite from Serra do Mar has a low content of Fe bearing primary minerals (Lelikov and Pirogova, 2009). Alternated layers of kaolin and organic material (Figure 3) suggest the occurrence of events with several pediplanation during the sediment deposition at the peatland areas. Morphological variations in soil particles, such as surface features and color transition (Figure 3), reveal a lithological discontinuity with materials deposited in distinct events, particularly on the sand fraction (Table 1) (Bong et al., 2012; Awad et al., 2018; Sharaka et al., 2022). Under past environmental conditions with wetter climate followed by dried conditions and erosive processes, it originated the kaolin, possibly in the flatter position of the relief in Serra do Mar. These pedogenetic processes continuously filled the basin, covering the peat formed in the colder past environment (Melo et al., 2020; Chiapini et al., 2020). Alternation of events favoured the continuous cycle of formation (primary) and deposition (secondary) of the kaolinite, resulting in the sedimentation of materials containing layers of peat and kaolinite over time. Larger contents of kaolin between peat layers are derived from erosion pulses, representing a long period of erosion and deposition of materials. The peat was formed after the fulfilling the valley (peatlands) and, as a flat and swampy terrain was formed, with limited drainage enabling the paludization process. Under humid environment with restricted drainage and continuous accumulation of organic matter, peat originated Histosols. Simultaneously to these events, the peat is buried by new layers of kaolin derived from erosion processes, highly contributing to the deposition of the coarser material at the foot of the slope, while the finer material (white clay) was gradually deposited in the peat. After successive landslides, the vegetation grows, and the paludization process restarts (Schellekens et al., 2009; Keaney et al., 2013).

Data from EDS analysis for the silt fraction revealed the highest mean $\text{SiO}_2/\text{Al}_2\text{O}_3$ ratio of mica-kaolinite pseudomorph particles for SAP samples (1.67 – Figure 6). Ideal kaolinite ratio of $\text{SiO}_2/\text{Al}_2\text{O}_3$ is 1.18 (chemical composition according to the ideal structural formula of kaolinite: 46.5 % SiO_2 , 39.5 % Al_2O_3 and 14 % H_2O) (Grumer, 1932; Brindley and Robinson, 1947). This higher ratio for SAP samples evidenced high amount of mica layers (2:1) inside the mica-kaolinite pseudomorph particles. The highest K content was also observed for this sample (Figure 6). On the other hand, the floodplain sediment layers are more weathered than the Serra do Mar saprolite (SAP), resulting in lower $\text{SiO}_2/\text{Al}_2\text{O}_3$ ratios. The 2:1 layer of mica forms two 1:1 layers of kaolinite, releasing K-interlayered but keeping the mica morphology (pseudomorph) (Muggler, 1998; Kämpf et al., 2009; Ekosse, 2010; Galán and Ferrell, 2013).

Presence of kaolinite-mica pseudomorphs in the silt fraction of all analysed samples (Figure 5) does not clarify the genesis of the lowland sedimentary layers. The three-genesis premises admit the presence of kaolinite-mica pseudomorphs in both Serra do Mar and peatland areas: i) kaolinite-mica pseudomorphs were formed in Serra do Mar and transported to the peatland area; ii) kaolinite-mica pseudomorphs are autochthonous in the peatland area, formed directly from the weathering of mica transported to the pediplain. The mean value of thickness (basal growth) of the pseudomorph, highlighted in sample C2-382, is approximately 30 μm and the particle highlighted in SAP is about half of this thickness (Figure 5), indicating *in situ* formation of the pseudomorph in silt fraction for the C2-382 samples, possibly by the weathering of the transported mica. In this deepest sediment lens, the pseudomorphs are more weathered (containing only kaolinite layers) and coarser than the same mineral in SAP; iii) combination of both processes: part of the kaolinite-mica pseudomorphs was transported, and part was formed *in situ* in the peatland.

Table 3. Crystallographic parameters of kaolinite in clay fraction

Sample	Plane	d	MCD	ms	HBCI	AI
		nm				
KL	(001)	0.722	11.0	2.19	13.7	0.075
	(020)	0.447		0.81		
	(002)	0.358		1.52		
	(200)	0.250	12.5	0.83		
	(060)	0.149	17.6	0.33		
SAP	(001)	0.720	10.0	2.33	12.2	0.213
	(020)	0.448		0.85		
	(002)	0.359		2.27		
	(200)	0.250	12.7	0.12		
	(060)	0.149	18.2	0.35		
C1-145	(001)	0.721	8.2	2.84	13.5	0.059
	(020)	0.447		0.62		
	(002)	0.358		1.80		
	(200)	0.250	16.8	1.02		
	(060)	0.149	14.5	0.42		
C1-172	(001)	0.722	7.8	2.78	8.4	0.129
	(020)	0.486		0.78		
	(002)	0.358		2.65		
	(200)	0.250	13.7	1.50		
	(060)	0.149	13.9	0.52		
C1-292	(001)	0.724	9.3	2.32	9.5	0.101
	(020)	0.486		0.41		
	(002)	0.358		1.20		
	(200)	0.250	19.8	1.33		
	(060)	0.149	16.9	0.47		
C2-130	(001)	0.720	9.0	2.88	11.3	0.100
	(020)	0.446		0.73		
	(002)	0.357		1.80		
	(200)	0.250	14.4	1.32		
	(060)	0.149	17.9	0.40		
C2-315	(001)	0.720	9.3	2.90	13.2	0.075
	(020)	0.447		0.30		
	(002)	0.358		2.02		
	(200)	0.250	16.1	1.23		
	(060)	0.149	16.9	0.44		
C2-382	(001)	0.720	13.1	2.30	12.8	0.055
	(020)	0.447		0.71		
	(002)	0.357		1.19		
	(200)	0.250	17.2	0.75		
	(060)		17.9	0.38		

DSAP: kaolinitic saprolite; KL: kaolinitic layer; d: interplanar spacing; MCD: mean crystal diameter; ms: microstrain in (060) plane; HBCI: Hughes and Brown crystallinity index; AI: asymmetry index.

In the KL (Serra do Mar) and peatland deposits area (C1 and C2), kaolinite in the clay fraction with higher AI (predominant 2:1 layers) showed poor crystallinity (lower HBCI) (Table 3), explained by the larger 2:1 interstratification (Simas et al., 2006; Oliveira Junior et al., 2014; Testoni et al., 2017). The taller AI observed for SAP than KL (Table 3)

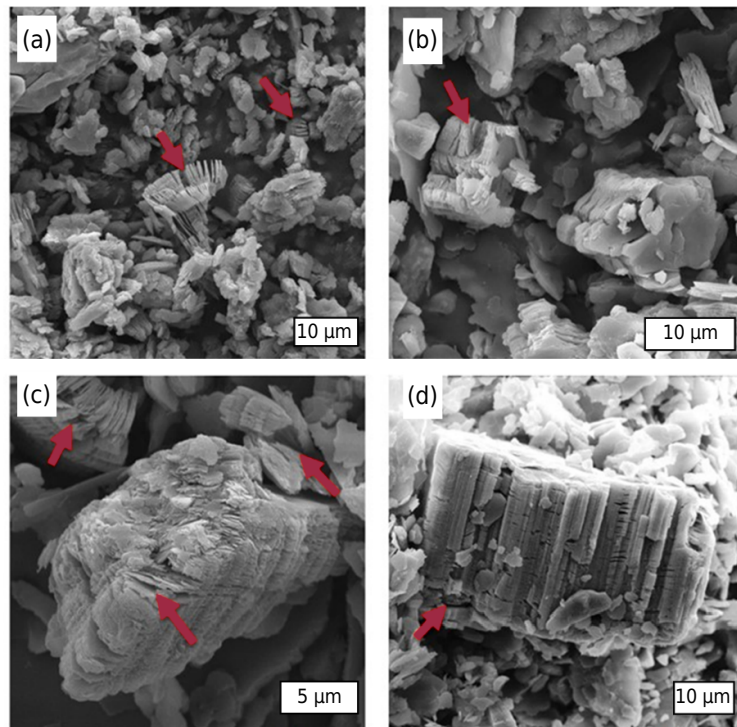


Figure 5. Scanning electron microscopy (SEM) images for silt fraction: (a) kaolinitic saprolite (SAP); (b) C1-292; (c) C2-315; and (d) C2-382 samples. Red arrows indicate the transformation of mica into kaolinite (pseudomorph).

revealed pedogenic differences between these materials, although both sites are located at Serra do Mar. Neogenesis from K-feldspar veins commonly present in migmatites for KL kaolinite is the main process (Oliveira et al., 2007) to reduce the Al of the mineral. The higher kaolinite content on KL than SAP (Table 2) evidenced the alteration of the K-feldspar vein, where the more heterogeneous clay mineralogy of SAP (Figure 5a) resulted in lower kaolinite contents and higher Al.

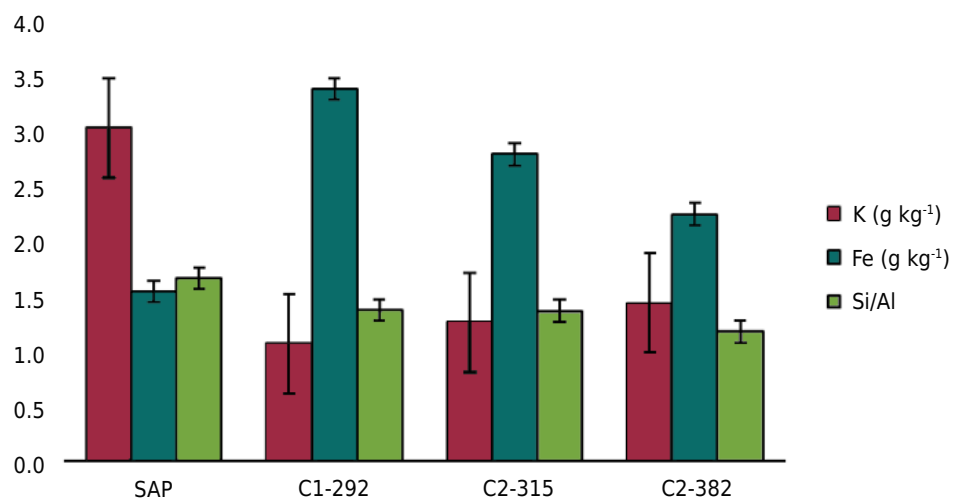


Figure 6. Standard deviation (black lines) and mean content (filled bar) of K, Fe, and $\text{SiO}_2/\text{Al}_2\text{O}_3$ ratio by EDS (energy dispersive X-ray spectroscopy) analysis for silt minerals (mica-kaolinite pseudomorphs) identified in figure 5 of SAP (five particles), C1-292 (five particles), C2-315 (nine particles) and C2-382 (ten particles).

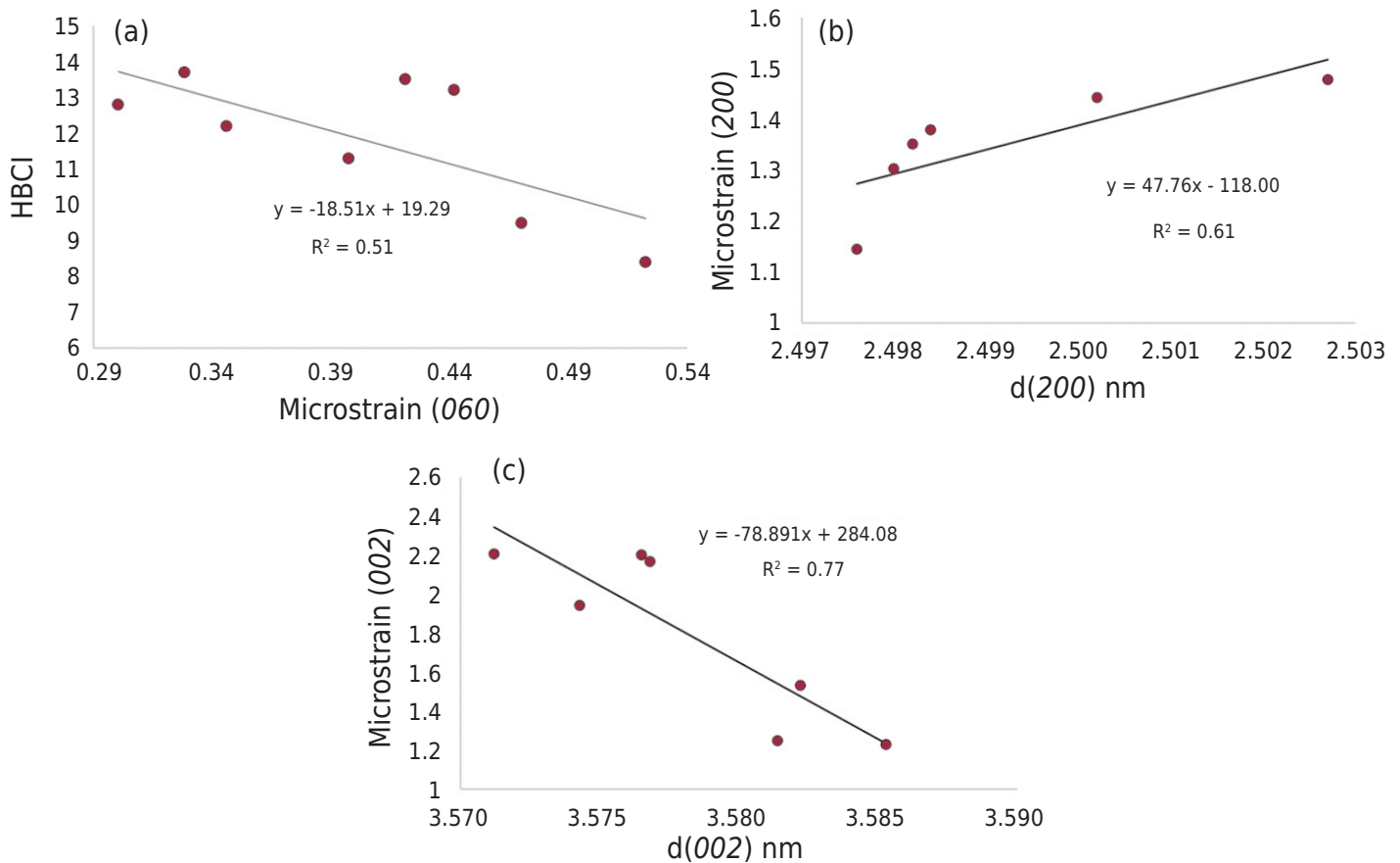


Figure 7. Correlation between crystallographic parameters of kaolinite in the clay fraction (values were shown in Table 3): (a) HBCI (Hughes and Brown crystallinity index) \times microstrain (060); (b) microstrain (002) \times $d(200)$; and (c) microstrain (002) \times $d(002)$.

The highest values of ms (structural strain measurement) for the (001) plane of kaolinite are due to increased isomorphous substitution (IS) of Al^{3+} by Fe^{3+} into the octahedral sheets (Harvey and Merino, 2016; Siebecker et al., 2018). The IS affects the unit cell parameters of kaolinite and deforms its crystalline structure (negative correlation between ms (060) and HBCI - Figure 7a). Despite the increasing dimensions of the unit cell in a and b crystal axes (Figure 7b), the IS into octahedral sheet reduced the kaolinite thickness (negative correlation between ms (002) and $d(002)$ - Figure 7c). When trivalent cations share two consecutive octahedral positions, electrostatic repulsions may occur in the crystal structure, elongating and shortening the shared edge. This process lead to the corrugation of the kaolinitic sheet, drastically reducing its thickness (Schaetzl and Anderson, 2005; Uddin, 2017).

Desilication is the main process to explain the variability of the clay fraction data. Higher degree of desilication increases gibbsite contents and the disorder of kaolinite (inverse positions of gibbsite contents and HBCI in PCA analysis - Figure 8a). Higher organic matter contents and stronger weathering conditions resulted in higher gibbsite contents and decreased kaolinite crystallinity in the peatland area. Normally, kaolinite particles from kaolin layers form and grow in purer environments, reducing possible interferences with foreign ions and organic material (Melo et al., 2001). In the purer environment (Serra do Mar), the SAP and KL were separated by the AI values (Figure 8a), and as previously discussed, a higher contribution of K-feldspar is assumed in the formation of kaolinite of the clay fraction of KL, which reduces the AI values.

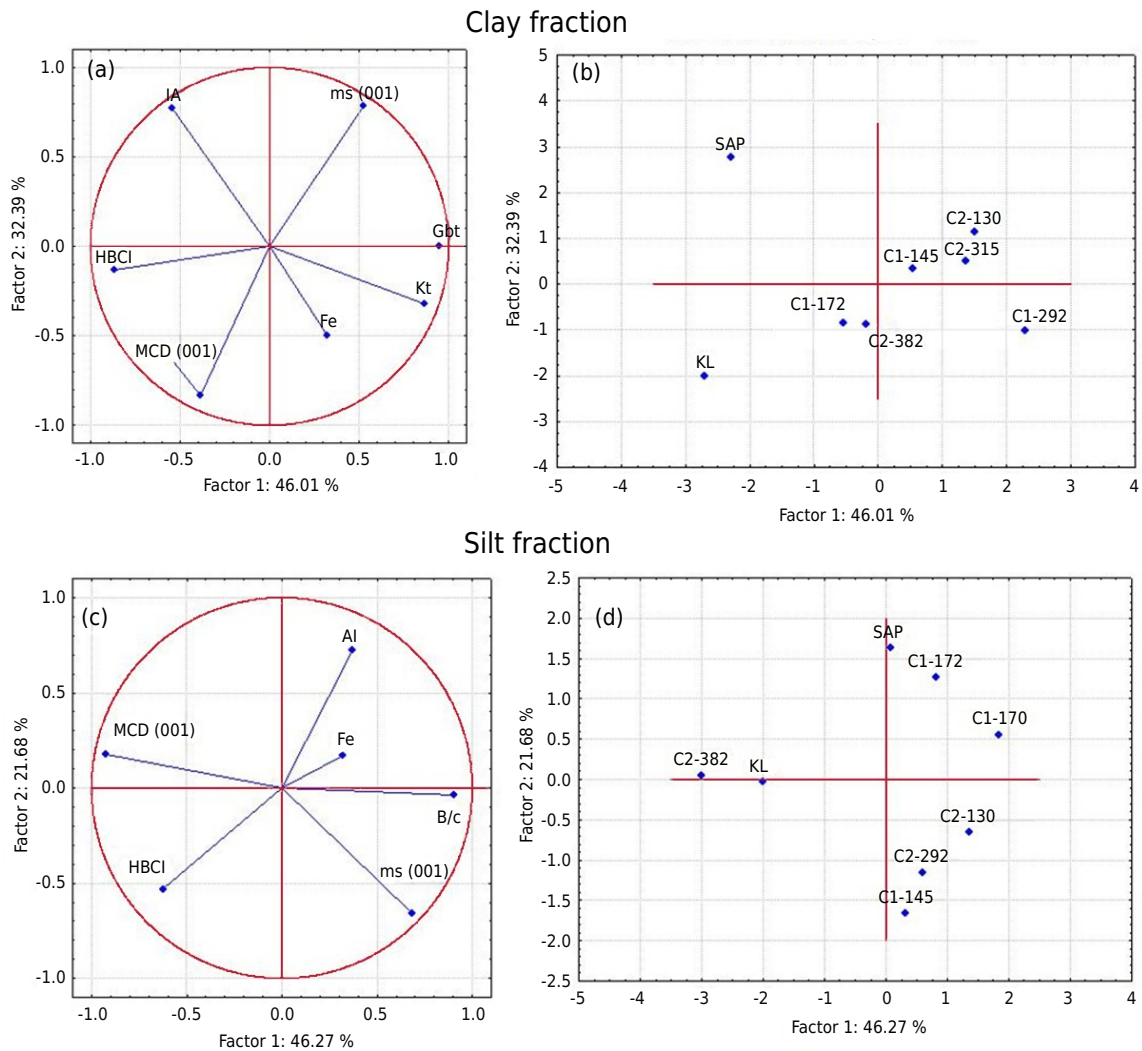


Figure 8. Principal component analysis of the clay (a, b); and silt fractions (c, d). Al: asymmetric index; MCD: mean crystal diameter; Gb: gibbsite; Kt: kaolinite, HBCI: Hughes and Brown crystallinity index; ms: microstrain; SAP: kaolinitic saprolite; and KL: kaolinitic layer on Serra do Mar.

Projection of the silt fraction in the factorial plane (Figure 8c) indicates that Serra do Mar samples were separated from peatland samples by their larger size of mica-kaolinite pseudomorph crystals in the basal and in the (060) planes. On the other hand, samples of the peatland area showed greater deformations in (060) plane. Within the peatland samples, C1 was separated from core 2 by its higher Al values and lower ms in (001) plane, except for the C1-145, which represent the same deposit layer from C2 (C2-130 and C2-315). Core 2 samples showed lower $\text{SiO}_2/\text{Al}_2\text{O}_3$ ratio (Figure 6), revealing lower contents of mica layers in pseudomorphs (lower Al values). The deepest C2 sample (C2-382) was placed in the same quadrant of KL sample, despite having a lower $\text{SiO}_2/\text{Al}_2\text{O}_3$ ratio (1.18) (therefore, fewer mica layers and lower Al). This behavior is due to their highest crystal growth (MCD) inherited from Serra do Mar deposits. Presence of minerals such as 2:1 with or without Al-hydroxy interlayered and mica pseudomorphs, among others, is relatively common in the clay fraction of soils, particularly forming interstratified with kaolinite. This randomized interstratification is well explained by the occurrence of highly heterogeneous environments with dissolution and precipitation reactions in the chemical equilibria of minerals. In this way, it is assumed that Al are strictly related to interstratifications, given the pedogenetic heterogeneity of the environments studied (Herbillon et al., 1981; Neumann et al., 2011; Testoni et al., 2017).

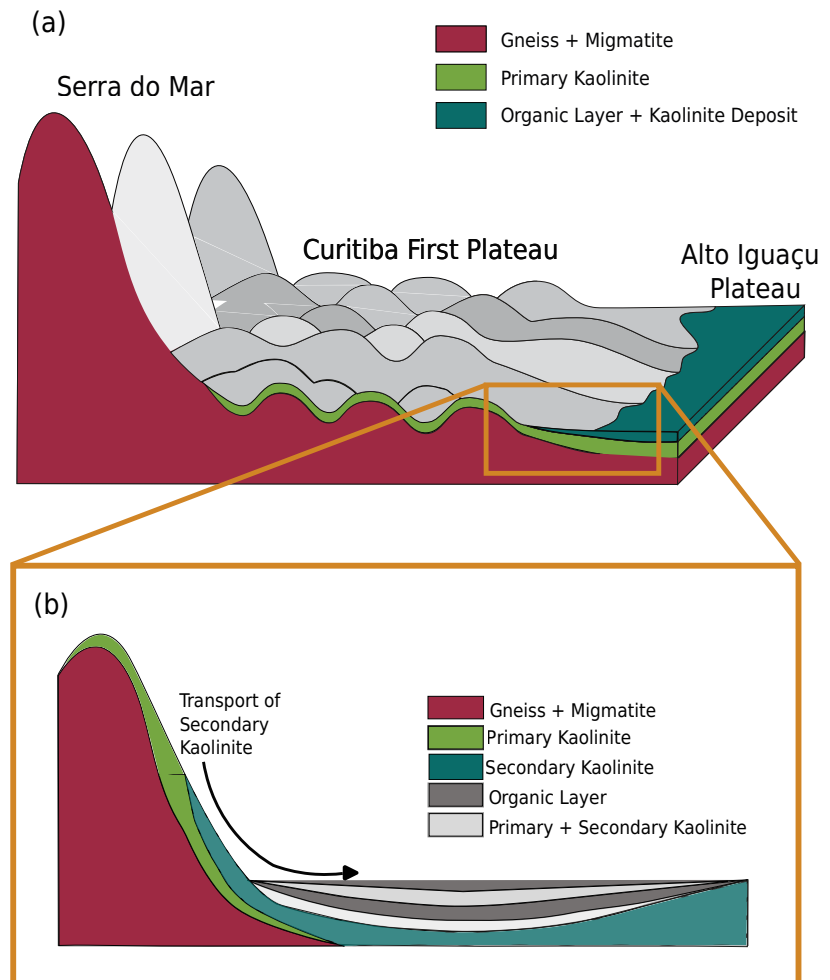


Figure 9. Model of geomorphology evolution and kaolinite in Serra do Mar and peatlands. (a) Geomorphological setting and the relation with Serra do Mar and peatland. (b) Origin of the primary and secondary kaolinite, the peat formation and mixture of primary and secondary kaolinite in the peatland.

CONCLUSIONS

Chemical and crystallographic characteristics of kaolinite can be divided according to the particle size and the location in the relief. 1) Silt fraction: i) Serra do Mar saprolite (SAP) – genesis mainly from mica weathering (primary kaolinite); ii) peatland – in general, the pseudomorph crystals are smaller than those of Serra do Mar, due to fragmentation along the transportation. 2) Clay fraction: i) Serra do Mar – there was a greater contribution of K-feldspar weathering; ii) peatland – the greater weathering of this landscape position resulted in poorly ordered kaolinites, due to the rich soil solution of neoformed kaolinite at the local (primary kaolinite). A combination of both genesis processes, where part of the kaolinite was transported (allochthonous material) from Serra do Mar and part was formed *in situ* in the peatland is assumed as the main process.

ACKNOWLEDGMENTS

Our most sincere thanks to Silmar Burer, the owner of Fazenda Boqueirão where cores were sampled, and to Serra do Caulim mineradora, where the Sea range samples were collected. We also would like thanks to Electronic Microscopy Center of Federal University of Paraná for SEM-EDS analyses, to the technician Maria Aparecida de Carvalho for helping in the mineralogical analysis in the Laboratory of Soil Mineralogy, Department of Soil Science, Federal University of Paraná and to the technician Dorival Grisotto for helping in the field work.

AUTHOR CONTRIBUTIONS

Conceptualization:  Jairo Calderari de Oliveira Junior (supporting) and  Vander de Freitas Melo (lead).

Data curation:  Daniela Nicole Ferreira (supporting),  Jairo Calderari de Oliveira Junior (lead),  Samara Alves Testoni (supporting) and  Vander de Freitas Melo (supporting).

Formal analysis:  Daniela Nicole Ferreira (equal),  Jairo Calderari de Oliveira Junior (equal),  Samara Alves Testoni (supporting) and  Vander de Freitas Melo (equal).

Funding acquisition:  Jairo Calderari de Oliveira Junior (supporting) and  Pablo Vidal-Torrado (lead).

Investigation:  Daniela Nicole Ferreira (equal),  Jairo Calderari de Oliveira Junior (equal),  Samara Alves Testoni (supporting) and  Vander de Freitas Melo (equal).

Methodology:  Jairo Calderari de Oliveira Junior (equal) and  Vander de Freitas Melo (equal).

Project administration:  Jairo Calderari de Oliveira Junior (lead).

Resources:  Jairo Calderari de Oliveira Junior (equal) and  Pablo Vidal-Torrado (equal).

Software:  Jairo Calderari de Oliveira Junior (lead).

Supervision:  Jairo Calderari de Oliveira Junior (lead).

Validation:  Jairo Calderari de Oliveira Junior (lead).

Visualization:  Daniela Nicole Ferreira (equal),  Jairo Calderari de Oliveira Junior (equal),  Pablo Vidal-Torrado (equal),  Samara Alves Testoni (supporting) and  Vander de Freitas Melo (equal).

Writing - original draft:  Daniela Nicole Ferreira (supporting),  Jairo Calderari de Oliveira Junior (equal),  Samara Alves Testoni (supporting) and  Vander de Freitas Melo (equal).

Writing - review & editing:  Jairo Calderari de Oliveira Junior (equal),  Samara Alves Testoni (supporting) and  Vander de Freitas Melo (equal).

REFERENCES

- Alvares CA, Stape L, Sentelhas PC, Gonc LDM, Sparovek G. Koppen's climate classification map for Brazil Clayton. *Meteorol Z.* 2014;22:711-28. <https://doi.org/10.1127/0941-2948/2013/0507>
- Awad ME, López-Galindo A, Sánchez-Espejo R, Sainz-Díaz CI, El-Rahmany MM, Viseras C. Crystallite size as a function of kaolinite structural order-disorder and kaolin chemical variability: Sedimentological implication. *Appl Clay Sci.* 2018;162:261-7. <https://doi.org/10.1016/j.clay.2018.06.027>
- Baioumy HM. Mineralogy and geochemistry of clay fractions from different saprolites, Egypt: Implications for the source of sedimentary kaolin deposits. *Russ Geol Geophys.* 2014;55:1367-78. <https://doi.org/10.1016/j.rgg.2014.11.001>
- Batista AH, Melo VF, Gilkes R, Roberts M. Identification of heavy metals in crystals of sand and silt fractions of soils by scanning electron microscopy (SEM EDS/WD-EPMA). *Rev Bras Cienc Solo.* 2018;42:e0170174. <https://doi.org/10.1590/18069657rbcs20170174>

- Bedassa G, Getaneh W, Hailu B. Geochemical and mineralogical evidence for the supergene origin of kaolin deposits - Central Main Ethiopian Rift. *J Afr Earth Sci.* 2019;149:143-53. <https://doi.org/10.1016/j.jafrearsci.2018.08.005>
- Biondi JC, Santos ER. Depósito de caulim de Tijucas do Sul (Mina Fazendinha, Tijucas do Sul - PR). *Rev Bras Geocienc.* 2004;34:243-52. <https://doi.org/10.25249/0375-7536.2004342243252>
- Bong WSK, Nakai I, Furuya S, Suzuki H, Abe Y, Osaka K, Matsumoto T, Itou M, Imai N, Ninomiya T. Development of heavy mineral and heavy element database of soil sediments in Japan using synchrotron radiation X-ray powder diffraction and high-energy (116 keV) X-ray fluorescence analysis: 1. Case study of Kofu and Chiba region. *Forensic Sci Int.* 2012;220:33-49. <https://doi.org/10.1016/j.forsciint.2012.01.024>
- Brindley GW, Robinson K. The structure of kaolinite. *Mineral Mag.* 1945;27:242-53. <https://doi.org/10.1180/minmag.1946.027.194.04>
- Campos AP, Farias VM. Caulim. In: Brasil, Agência Nacional de Mineração. Sumário Mineral 2017. Brasília, DF: ANM; 2017. p. 78-80.
- Chen P-Y, Lin M-L, Zheng Z. On the origin of the name kaolin and the kaolin deposits of the Kauling and Dazhou areas, Kiangsi, China. *Appl Clay Sci.* 1997;12:1-25. [https://doi.org/10.1016/S0169-1317\(97\)00007-0](https://doi.org/10.1016/S0169-1317(97)00007-0)
- Chiapini M, Oliveira Junior JC, Schellekens J, Almeida JA, Buurman P, Vidal-Torrado P. Sombric-like horizon and xanthization in polychrome subtropical soils from Southern Brazil: Implications for soil classification. *Sci Agric.* 2020;78:e20190115. <https://doi.org/10.1590/1678-992x-2019-0115>
- Ciotta MN, Bayer C, Fontoura SMV, Ernani PR, Albuquerque JA. Matéria orgânica e aumento da capacidade de troca de cátions em solo com argila de atividade baixa sob plantio direto. *Cienc Rural.* 2003;33:1161-4. <https://doi.org/10.1590/s0103-84782003000600026>
- Departamento Nacional de Produção Mineral – Ministério de Minas e Energia. Boletim do Setor Mineral. Brasília, DF: Secretaria de Geologia, Mineração e Transformação Mineral; 2021.
- Dill HG, Bosse HR, Henning KH, Fricke A, Ahrendt H. Mineralogical and chemical variations in hypogene and supergene kaolin deposits in a mobile fold belt the Central Andes of northwestern Peru. *Miner Deposita.* 1997;32:149-63. <https://doi.org/10.1007/s001260050081>
- Driese SG, Medaris LG, Ren M, Runkel AC, Langford RP. Differentiating pedogenesis from diagenesis in early terrestrial paleoweathering surfaces formed on granitic composition parent materials. *J Geol.* 2007;115:387-406. <https://doi.org/10.1086/518048>
- Ekosse GIE. Kaolin deposits and occurrences in Africa: Geology, mineralogy and utilization. *Appl Clay Sci.* 2010;50:212-36. <https://doi.org/10.1016/j.clay.2010.08.003>
- Galán E, Ferrell RE. Genesis of clay minerals. *Dev Clay Sci.* 2013;5:83-126. <https://doi.org/10.1016/B978-0-08-098258-8.00003-1>
- Gaudin A, Ansan V, Lorand JP, Pont S. Genesis of a florencite-bearing kaolin deposit on ordovician schists at Saint-Aubin-des-Châteaux, Armorican Massif, France. *Ore Geol Rev.* 2020;120:103445. <https://doi.org/10.1016/j.oregeorev.2020.103445>
- Gee GW, Bauder JW. Particle size analysis by hydrometer: A simplified method for routine textural analysis and a sensitivity test of measurement parameters. *Soil Sci Soc Am J.* 1979;43:1004-7. <https://doi.org/10.2136/sssaj1979.03615995004300050038x>
- Gilg HA, Weber B, Kasbohm J, Frei R. Isotope geochemistry and origin of illite-smectite and kaolinite from the Seilitz and Kemmlitz kaolin deposits, Saxony, Germany. *Clay Miner.* 2003;38:95-112. <https://doi.org/10.1180/0009855033810081>
- Górniak K. The role of diagenesis in the formation of kaolinite raw materials in the Santonian sediments of the North-Sudetic Trough (Lower Silesia, Poland). *Appl Clay Sci.* 1997;12:313-28. [https://doi.org/10.1016/S0169-1317\(97\)00015-X](https://doi.org/10.1016/S0169-1317(97)00015-X)
- Grumer JW. The crystal structure of kaolinite. *Z Krist-Cryst Mater.* 1932;83:75-80. <https://doi.org/10.1524/zkri.1932.83.1.75>

- Harvey CC, Merino E. Hydrochemical factors influencing the crystallinity and composition of kaolins and other silicates, revisited. *Appl Clay Sci.* 2016;131:71-3. <https://doi.org/10.1016/j.clay.2016.01.028>
- Herbillon AJ, Frankart R, Vielvoye L. An occurrence of interstratified kaolinite-smectite minerals in a red-black soil toposequence. *Clay Miner.* 1981;16:195-201. <https://doi.org/10.1180/claymin.1981.016.2.07>
- Hinckley DN. Variability in "crystallinity" values among the kaolin deposits of the coastal plain of Georgia and South Carolina. *Clay Clay Miner.* 1962;11:229-35. <https://doi.org/10.1346/ccmn.1962.0110122>
- Hughes JC, Brown GA. A crystallinity index for soil kaolinite and its relation to parent rock, climate and soil maturity. *J Soil Sci.* 1979;30:557-63. <https://doi.org/10.1111/j.1365-2389.1979.tb01009.x>
- Ismail S, Husain V, Anjum S. Mineralogy and genesis of nagar parker kaolin deposits, tharparkar District, Sindh, Pakistan. *Int J Econ Environ Geol.* 2019;5:33-40. <https://doi.org/10.46660/IJEEG.VOL0.ISS0.0.109>
- Jackson ML. *Soil chemical analysis: Advanced course.* Madison: Prentice-Hall; 1979.
- Kämpf N, Curi N, Marques JJ. Intemperismo e ocorrência de minerais no ambiente do solo. In: Melo VF, Alleoni LRF, editors. *Química e mineralogia do solo. Parte I – Conceitos básicos.* Viçosa, MG: Sociedade Brasileira de Ciência do Solo; 2009. p. 333-80.
- Karakaya MÇ, Karakaya N, Temel A, Yavuz F. Mineralogical and geochemical properties and genesis of kaolin and alunite deposits SE of Aksaray (Central Turkey). *Appl Geochem.* 2021;124:104830. <https://doi.org/10.1016/j.apgeochem.2020.104830>
- Keaney A, McKinley J, Graham C, Robinson M, Ruffell A. Spatial statistics to estimate peat thickness using airborne radiometric data. *Spat Stat.* 2013;5:3-24. <https://doi.org/10.1016/j.spasta.2013.05.003>
- Klug HP, Alexander LE. *X-ray diffraction procedures.* 2nd. ed. New York: John Wiley; 1974.
- Lelikov YP, Pirogova LG. Petrochemical and geochemical characteristics of a migmatite gneiss complex in the Southwestern sea of Japan. *Int Geol Rev.* 1978;20:947-54. <https://doi.org/10.1080/00206817809471548>
- Mártires RAC. Caulim. In: Brasil, Departamento Nacional de Produção Mineral. *Sumário Mineral 2006.* Brasília, DF: DNPM/DIDEM; 2006. p. 79-83.
- Mehra OP, Jackson ML. Iron oxide removal from soils and clays by a dithionite-citrate system buffered with sodium bicarbonate. *Clay Clay Miner.* 1958;7:317-27. <https://doi.org/10.1346/CCMN.1958.0070122>
- Melo VF, Singh B, Schaefer CEGR, Novais RF, Fontes MPF. Chemical and mineralogical properties of kaolinite-rich Brazilian soils. *Soil Sci Soc Am J.* 2001;65:1324-33. <https://doi.org/10.2136/sssaj2001.6541324x>
- Melo VF, Oliveira Junior JC de, Batista AH, Cherobim VF, Favaretto N. Goethite and hematite in bichromic soil profiles of southern Brazil: Xanthization or yellowing process. *Catena.* 2020;188:104445. <https://doi.org/10.1016/j.catena.2019.104445>
- Montes CR, Melfi AJ, Carvalho A, Vieira-Coelho AC, Formoso MLL. Genesis, mineralogy and geochemistry of kaolin deposits of the Jari river, Amapá State, Brazil. *Clay Clay Miner.* 2002;50:494-503. <https://doi.org/10.1346/000986002320514217>
- Mucha NM. *Relação solo-relevo entre a Serra do Mar e Planalto do Alto Iguaçu como subsídio para o mapeamento digital de solos [dissertation].* Curitiba: Universidade Federal do Paraná; 2020.
- Muggler CC. *Polygenetic Oxisoil on tertiary surfaces, Minas Gerais, Brazil: Soil genesis and landscape development [dissertation].* Wageningen: Wageningen Agricultural University; 1998.
- Neumann R, Costa GEL, Gaspar JC, Palmieri M, Silva SEE. The mineral phase quantification of vermiculite and interstratified clay minerals-containing ores by X-ray diffraction and Rietveld

- method after K cation exchange. *Miner Eng.* 2011;24:1323-34. <https://doi.org/10.1016/j.mineng.2011.05.017>
- Oliveira Junior JC, Melo VF, Souza LCP, Rocha HO. Terrain attributes and spatial distribution of soil mineralogical attributes. *Geoderma.* 2014;213:214-25. <https://doi.org/10.1016/j.geoderma.2013.08.020>
- Oliveira Junior JC, Souza LCP, Melo VF. Variability of soil physical and chemical properties in different plot divisions of the Guabirotuba formation. *Rev Bras Cienc Solo.* 2010;34:1491-502. <https://doi.org/10.1590/S0100-06832010000500002>
- Oliveira MTG, Furtado SMA, Formoso MLL, Eggleton RA, Dani N. Coexistence of halloysite and kaolinite - A study on the genesis of kaolin clays of Campo Alegre Basin, Santa Catarina State, Brazil. *An Acad Bras Cienc.* 2007;79:665-81. <https://doi.org/10.1590/s0001-37652007000400008>
- Ouyang N, Zhang Y, Sheng H, Zhou Q, Huang Y, Yu Z. Clay mineral composition of upland soils and its implication for pedogenesis and soil taxonomy in subtropical China. *Sci Rep.* 2021;11:9707. <https://doi.org/10.1038/s41598-021-89049-y>
- Pruett RJ. Kaolin deposits and their uses: Northern Brazil and Georgia, USA. *Appl Clay Sci.* 2016;131:3-13. <https://doi.org/10.1016/j.clay.2016.01.048>
- Salamuni E, Ebert HD, Borges MS, Hasui Y, Costa JBS, Salamuni R. Tectonics and sedimentation in the Curitiba Basin, south of Brazil. *J South Am Earth Sci.* 2003;15:901-10. [https://doi.org/10.1016/S0895-9811\(03\)00013-0](https://doi.org/10.1016/S0895-9811(03)00013-0)
- Santos HG, Jacomine PKT, Anjos LHC, Oliveira VA, Lumbrreras JF, Coelho MR, Almeida JA, Araújo Filho JC, Oliveira JB, Cunha TJF. Sistema brasileiro de classificação de solos. 5. ed. rev. ampl. [e-book]. Brasília, DF: Embrapa; 2018.
- Sayin A. Origin of kaolin deposits: Evidence from the Hisarcik (Emet-Kütahya) deposits, western Turkey. *Turkish J Earth Sci.* 2007;16:77-96.
- Schaetzl RJ, Anderson S. *Soils: Genesis and geomorphology.* Cambridge: Cambridge University Press; 2005.
- Schellekens J, Buurman P, Pontevedra-Pombal X. Selecting parameters for the environmental interpretation of peat molecular chemistry - A pyrolysis-GC/MS study. *Org Geochem.* 2009;40:678-91. <https://doi.org/10.1016/j.orggeochem.2009.03.006>
- Sharaka HK, El-Desoky HM, Abd El Moghny MW, Abdel Hafez NA, Saad SAA. Mineralogy and lithogeochemistry of lower Cretaceous kaolin deposits in the Malha Formation, Southwestern Sinai, Egypt: Implications for the building and construction industry. *J Asian Earth Sci X.* 2022;7:100087. <https://doi.org/10.1016/j.jaesx.2022.100087>
- Siebecker MG, Chaney RL, Sparks DL. Natural speciation of nickel at the micrometer scale in serpentine (ultramafic) topsoils using microfocused X-ray fluorescence, diffraction, and absorption. *Geochem Trans.* 2018;19:14. <https://doi.org/10.1186/s12932-018-0059-2>
- Simas FNB, Schaefer CEGR, Melo VF, Guerra MBB, Saunders M, Gilkes RJ, Sayin SA, Vieira KTP, Fernandes LA, Wilson IR, Santos HS, Santos PS. Clay-sized minerals in permafrost-affected soils (Cryosols) from King George Island, Antarctica. *Clay Clay Miner.* 2006;54:721-36. <https://doi.org/10.1346/CCMN.2006.0540607>
- Testoni SA, Almeida JA de, Silva L da, Andrade GRP. Clay mineralogy of Brazilian Oxisols with shrinkage properties. *Rev Bras Cienc Solo.* 2017;41:e0160487. <https://doi.org/10.1590/18069657rbcs20160487>
- Uddin MK. A Review on the adsorption of heavy metals by clay minerals with special focus on the past decades. *Chem Eng J.* 2017;308:418-62. <https://doi.org/10.1016/j.cej.2016.09.029>
- Vieira KTP, Fernandes LA. Análise faciológica e contexto deposicional do geossítio Bacia Sedimentar de Curitiba, nova seção-tipo para a Formação Guabirotuba. *Geol USP Série Científica.* 2020;20:87-104. <https://doi.org/10.11606/issn.2316-9095.v20-165568>
- Whittig LD, Allardice WR. X-ray diffraction techniques. In: Klute A, editor. *Methods of soil analysis: Part 1 - Physical and mineralogical methods.* 2nd. ed. 1965. p. 374-90. <https://doi.org/10.2136/sssabookser5.1.2ed.c12>